Journal of Manufacturing Processes 57 (2020) 905–918

Contents lists available at ScienceDirect

Journal of Manufacturing Processes

journal homepage: www.elsevier.com/locate/manpro

Technical Paper

Thermomechanical analysis of additively manufactured bimetallic tools for hot stamping

Magdalena Cortina*, Jon Iñaki Arrizubieta, Jose Exequiel Ruiz, Aitzol Lamikiz

Department of Mechanical Engineering, University of the Basque Country (UPV/EHU), Bilbao, Spain

ARTICLE INFO

Keywords:
Directed Energy Deposition
Laser cladding
Functional coating
Hot stamping
Bimetallic
Cycle time

ABSTRACT

A comparison between a conventional AISI H13 hot stamping tool and a bimetallic tool consisting of an AISI 1045 core and a laser-deposited AISI H13 coating is performed. In order to analyze the performance of bimetallic tools, the material compatibility and quality of the coating are analyzed. Besides, the mechanical properties are evaluated and compared with those of the conventional tool, obtaining mechanically equivalent results.

Nevertheless, the real conductivity of the laser deposited AISI H13 is found to be 16 % lower than the theoretical value. Hence, a thermal model of the hot stamping process is developed, and the performance of various coating thicknesses is evaluated. Results show that, in the present case study, an AISI 1045 tool with a 1 mm AISI H13 coating ensures the mechanical properties and reduces the cycle time by 44.5 % when compared to a conventional AISI H13 tool.

Introduction to DED in hot stamping

Hot stamping process

Growing demand in the automotive industry for high strength and lightweight components has driven the development of hot stamping (also known as press hardening) processes [1]. This circumstance is due to stricter CO_2 emission regulations forcing the industry to seek ways to build lightweight, more fuel-efficient cars. At the same time, car-safety improvement is demanded by both customers and legislation [2].

Through hot stamping, a boron steel blank is heated above the austenitic temperature, between 900 °C and 950 °C, in a furnace and then transferred to an internally cooled tool set, where it is simultaneously formed and quenched. Due to the high formability of the blank at high temperatures, this process enables the attainment of complex geometries. The total cycle time, including transfer, stamping, and quenching, takes 15–25 s [3]. The transformation of austenite into martensite occurs thanks to the rapid cooling of the blank, at a temperature range of 420–280 °C, along which the tools must be actively cooled at rates above 27 $°C{\cdot}s^{-1}$ [4]. As a result, a fully martensitic microstructure is achieved, providing the final part with an ultra-high-strength up to 1500 MPa [5].

Hot stamping is a process in which tooling is a key element. This is because stamping dies are high-added-value components with increased manufacturing and maintenance costs, and, besides, they strongly influence the characteristics of the final product [6]. In hot stamping, attainable productivity is closely related to the cooling time until the blank undergoes the martensitic transformation [7]. This stage is the longest one within the hot stamping process and consumes more than 30 % of the total cycle time [8]. In this regard, both the material thermal properties and the die cooling system play a key role [9]. Any improvement in those elements aiming to increase heat transfer between the tools and the stamped part would lead to higher production rates.

Parameters involved in the cooling process

The capacity of the hot stamping tools to dissipate heat from the blank is defined by means of three factors, which are the Convective Heat Transfer (CHTC), the Interfacial Heat Transfer Coefficient (IHTC) and the thermo-physical properties of the tool material.

On the one hand, the CHTC defines the capability of the cooling channels to extract the heat from the stamping tools, which is usually characterized by forced convection of water through the internal cooling channels. The CHTC is defined according to Eq. (1) [10], where k is the thermal conductivity of water, Nu the Nusselt number, and D the diameter of the channel.

* Corresponding author.
E-mail addresses: magdalena.cortina@ehu.eus (M. Cortina), joninaki.arrizubieta@ehu.eus (J.I. Arrizubieta), joseexequiel.ruiz@ehu.eus (J.E. Ruiz), aitzol.lamikiz@ehu.eus (A. Lamikiz).

https://doi.org/10.1016/j.jmapro.2020.07.036
Received 21 October 2019; Received in revised form 17 July 2020; Accepted 22 July 2020
Available online 06 August 2020

$$CHTC = \frac{k \cdot Nu}{D} \quad (1)$$

On the other hand, the IHTC is a thermo-physical parameter indicating the heat transferability between the interfaces of the hot blank and the cold die. This parameter has a strong influence on the temperature distribution in the blank, therefore affecting the final characteristics of the hot-stamped part. Some of the factors influencing the IHTC are: (1) the topography at the interface, (2) the contact pressure, (3) the temperature of blank and tool, and (4) the thermo-physical properties of the tool material [16]. In fact, Chang et al. concluded in their research that the thermal conductivity and the specific heat capacity are the main thermo-physical properties influencing the IHTC [16].

Once a good contact between the blank and the tool is guaranteed, and the water flow through the cooling system is turbulent enough, the thermo-physical properties of the tool material determine the heat transfer between the blank and the tool [14]. Among the different thermo-physical properties, any modification of the thermal conductivity results in significant variations of the thermal capacity of the tools. Moreover, as it is highlighted in Fig. 1, the improvement of the total effective thermal conductivity of the tools implies also an improvement in the other two factors.

Research in this field

In this direction and regarding the optimization of hot stamping tools, different research fields have been explored, such as the use of high conductivity steels [11] or the integration of conformal channels within the stamping tools [12] and their design optimization [13].

Hot work tool steels, such as AISI H13, have been generally used for manufacturing hot stamping dies. Their excellent mechanical properties at high temperatures make them stand out among other materials; however, they have moderate thermal conductivity values that remain between 25–30 $W \cdot m^{-1} K^{-1}$. In order to take advantage of this issue, tool steel grades with high surface hardness and improved thermal conductivity have been developed, attaining values of up to 60 $W \cdot m^{-1} K^{-1}$ and thus enabling a cycle-time reduction of 35–45 % [15]. Ghiotti et al. analyzed the tribological behavior of two high thermal conductivity steel grades in terms of friction and wear damage. When compared with AISI H11, both high thermal conductivity steels showed a lower friction coefficient and subsequent lower resistance to sliding. However, they presented larger abrasion, especially at high temperatures. Consequently, the impact of wear phenomenon on tool life may be significantly greater [11].

Components made of tool steels are quite expensive due to both material and manufacturing costs. In addition, in the case of hot stamping, higher conductivities are desirable. Chang et al. studied the thermal differences when using AISI 1045 and AISI H13 tools for stamping 22MnB5 blanks [16]. Therefore, hot stamping is an application where it is advantageous to manufacture tools using inexpensive, easy-to-fabricate steels, with their surface properties enhanced by coating with highly alloyed steels [17]. In this regard, laser-based additive processes have arisen as a key element for manufacturing high-performance tools at lower costs [18].

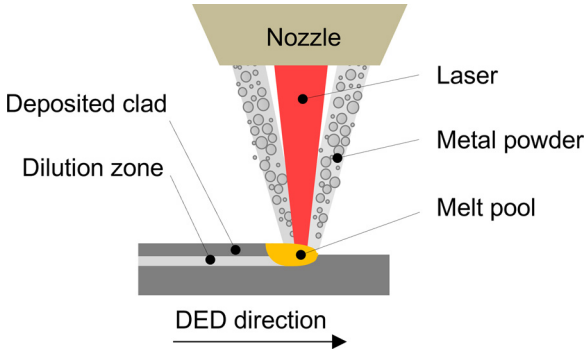

Fig. 2. Directed Energy Deposition working principle.

Among the different additive manufacturing (AM) technologies available, the Directed Energy Deposition (DED) processes have emerged as an alternative to traditional coating techniques that are gaining the attention of both academia and industry due to their repair and manufacturing applications [19]. DED consists of building a part by means of focusing thermal energy (e.g., laser, plasma arc, or electron beam) that simultaneously heats and melts a substrate while filler material in the form of powder or wire is injected into the melt pool [20], as shown in Fig. 2. The filler material is melted by the laser beam and bonded to the substrate, forming subsequent clads and layers until the required geometry is attained. In this way, the DED technologies enable the fabrication of fully dense near-net-shape parts with high-quality metallurgical bonding to the substrate [21].

The DED processes are employed for generating new geometries, as well as for repairing or applying coatings to pre-existing components [22], where the geometry of the deposited material needs to be controlled [23]. Besides, the DED process is frequently combined with subtractive technologies, such as milling [24]. The application fields of this technology are focused on the manufacturing and repair of high-added-value parts [25] intended for diverse industrial sectors such as aerospace [26], automotive, energy, medical, and die & mold [27].

Some research has been carried out in this area in the field of high-pressure die-casting. Aiming to develop higher thermal conductivity tools, Imran et al. presented an approach to replace a conventional steel die by a bimetallic die made of a copper alloy and coated with a protective AISI H13 layer using DED. In this way, the interaction between copper and aluminum, which have a strong chemical affinity, is avoided. As a result, they obtained a metallurgically sound and fully dense coating and were able to manufacture bimetallic dies with superior thermal performance, thus reducing the solidification time of aluminum by more than 30 % of the time required with conventional dies [28]. Nevertheless, copper is a difficult material to use in laser-based AM due to its high reflectivity index. Besides, the materials employed in hot stamping need to withstand high pressures, ranging

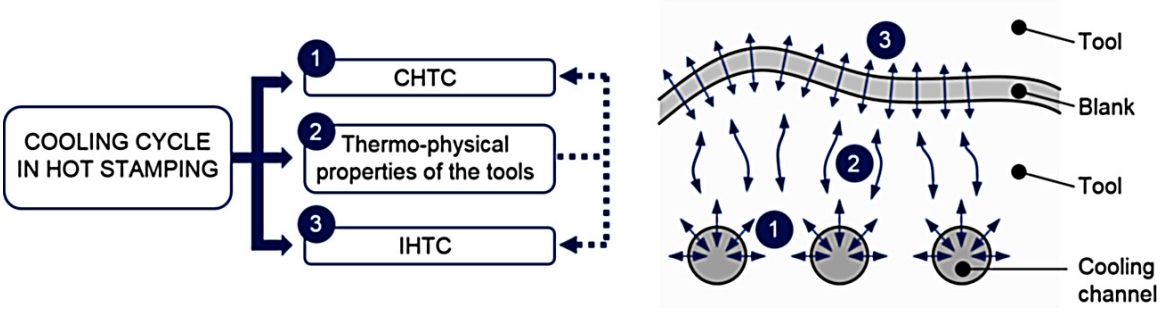

Fig. 1. Factors influencing the cooling cycle in hot stamping and a scheme of the heat transfer between the blank, tools, and cooling channels.

between 10–15 MPa [12,29,30], values that copper would be unable to withstand.

Hu et al. deposited CPM 10 V and CPM 15 V high-vanadium steel powders on AISI 1045 medium carbon steel aimed at manufacturing cutting and stamping dies. Sound clads free of porosity and cracks were attained, with an as-clad hardness of 650 HV, which is a similar value to that of heat-treated AISI D2. In fact, the authors claim that results could be used for cost-effective die manufacturing by replacing the expensive tool steel die blocks by ordinary structural steel [31]. In the same direction, Ocelík et al. coated AISI 1045 steel with Cr-Mo-W-V alloyed steel that shows enhanced properties, such as high wear resistance and compressive strength, good toughness, dimensional stability and tempering resistance. They attained homogeneous, defect-free coatings with good bonding to the substrate material and properties in terms of hardness, toughness, and wear resistance [32]. In order to improve the wear resistance of tool steels, Navas et al. studied the application of laser cladded protective coatings to repair AISI A2 cold work tool steel, commonly used in stamping tools, with AISI M2 high-speed steel and AISI 431 stainless steel. They found that wear resistance in unlubricated conditions was significantly improved with AISI M2, which shows a better performance than AISI 431, especially at high loads. This is attributed to the finer microstructure of AISI M2 and to the presence of carbides, which protect the material matrix from being worn [33]. With regard to repairing hot work tool steels, Kattire et al. deposited CPM 9 V high-vanadium tool steel on AISI H13, aiming at die restoration applications. The generated clads showed a hardness of about four times greater than the substrate hardness and compressive residual stresses, which would prevent cracks from propagating, thus enhancing the service life of dies [34].

From the literature review, it is noted that some research has been devoted to the field of repairing or improving the properties of tool steels. However, no work focusing on manufacturing cost-effective hot stamping tools can be found. Although bimetallic tools can be more complex and expensive, two major advantages are introduced. On the one hand, the material cost is reduced, since a much less amount of tool steel is required for coating the component, while the core of the die is made of a lower-cost conventional steel. On the other hand, the effective thermal conductivity of the die is increased, which reduces the cooling time of the part inside the stamping tool. Given the interest in the advantages of using bimetallic tools, it is necessary to assess the suitability of employing the DED technology to generate hot stamping tools. First, the quality of the deposited material is evaluated. Then, the resulting mechanical and thermal properties are also analyzed. Finally, and once the bimetallic tools are adequately studied and their correct performance is ensured, the real advantages in terms of productivity enhancement that they offer when compared with conventional tools are quantified.

Material and methods

Proposed methodology

The main objective of the present research work was to evaluate the suitability of additively manufactured bimetallic hot stamping tools and determine the advantages that the material combination offers. For this purpose, the methodology shown in Fig. 3 was employed:

(1) AM of AISI H13 tool steel over AISI 1045 conventional steel and study of the deposited material's quality considering several aspects: dilution, proper bonding between layers, porosity generation, and microstructure.
(2) Hardness was measured both superficially and in the cross-section of the sample; that is, at different depths across the deposited layers, finally reaching the substrate. In this way, the variation of hardness as a function of depth could be analyzed. Obtained values were compared with reference hardness measured on a cast AISI H13 block.
(3) In hot stamping, wear is the main factor affecting the service life and maintenance needs of tools. In order to investigate the tribological behavior of the deposited AISI H13 tool steel, a pin-on-disk test was performed. The same test was conducted over a cast AISI H13 block so that a reference wear value was attained, and a comparison between results could be made. In addition, the friction coefficient was also determined.
(4) Stamping tools must withstand the forces applied by the press and their subsequent contact pressures. In this regard, and in order to mechanically validate the bimetallic tool, compression tests were performed. Different AISI H13 coating thicknesses were tested, and results were compared with those of the reference AISI H13 tool steel material.
(5) In order to determine the real diffusivity of the laser-deposited AISI H13, its effective thermal diffusivity was measured by means of the flash method. Obtained results allowed the thermal model to be fed with the real thermal conductivity value of the deposited AISI H13.
(6) An analysis of the cycle-time reduction was performed by means of thermal modelling of the hot stamping process. Different AISI H13 coating thicknesses are analyzed, and, additionally, the evolution of hot spots and temperature variations in the stamped blank were evaluated.

Employed materials

In the experimental tests, AISI 1045 (DIN 1.1191) and AISI H13 (DIN 1.2344) were used as the base and filler materials, respectively. AISI 1045 is a medium-carbon steel commonly used in structural parts requiring high strength and hardness. AISI H13 is a Cr-MoV alloyed tool steel with a high level of resistance to thermal shock and fatigue and good temperature strength, qualities which make AISI H13 particularly valuable for tooling [35]. The filler material was supplied by Flame Spray Technologies and obtained via gas atomization, consisting of spherical particles with diameters of 53-150 μm. The chemical compositions of the employed materials are listed in Table 1.

Experimental procedure

DED tests

The DED experiments described in this work were performed on a 5-axis laser-processing machine, with a work-piece size capacity of 700 × 360 × 380 mm^3. A highpower Yb:YAG fiber laser source, Rofin FL010, with a maximum power output of 1 kW and emitting wavelength of 1070 nm was employed. In addition, the powder filler material was fed by means of a Sulzer Metco Twin 10-C powder feeder and an in-house designed coaxial nozzle [38], using argon as both the drag and shielding gasses.

In order to evaluate the quality of the deposition of AISI H13 over AISI 1045, coatings of approximately 7 mm height were deposited using the process parameters detailed in Table 2. The build-up strategy selected was a zigzag pattern, alternating longitudinal and transversal directions for the deposition of successive layers. The deposition direction was switched 90° between consecutive layers. Following the same procedure, coatings of 1, 3 and 5 mm height were also deposited over a 200 × 120 × 40 mm^3 substrate, enabling further analyzes.

Metallographic and hardness analysis

For metallographic analysis, five different cross-sections were extracted, polished, and etched using Marble reagent, so that their macro- and microstructure were revealed. After that, they were analyzed by using the Leica DCM3D microscope. The images acquired were used both for identifying internal defects within the deposited material and for performing a porosity analysis.

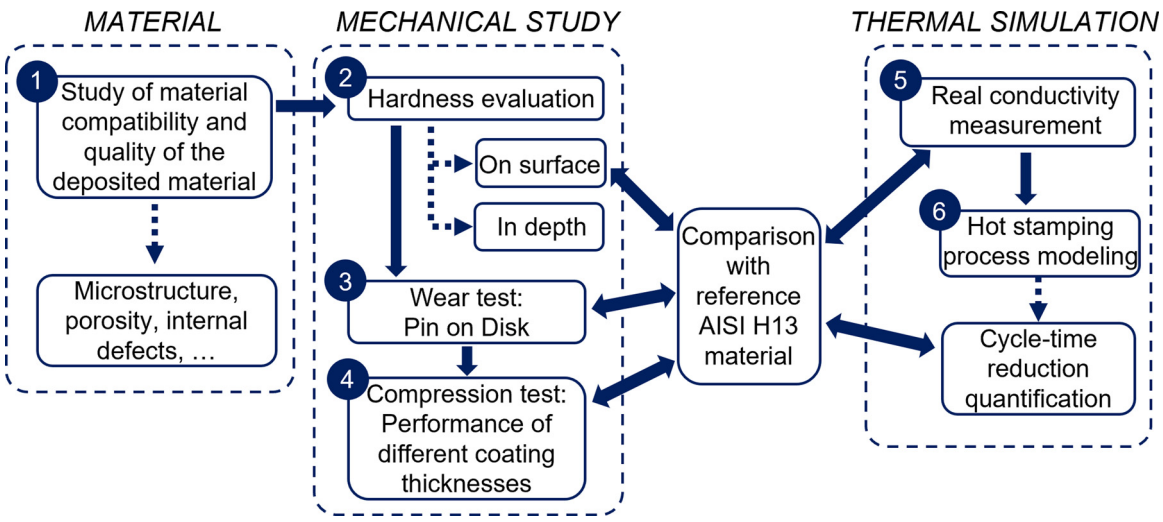

Fig. 3. Diagram of the employed methodology.

Table 1
Chemical composition (wt.%) of AISI 1045 [36] and AISI H13 [37].

Material	C	Si	Mn	Cr	Mo	V	Fe
AISI 1045	0.45	0.24	0.8	0.16	-	0.02	Balance
AISI H13	0.41	0.80	0.25	5.12	1.33	1.13	Balance

Table 2
Process parameters employed for the deposition of AISI H13.

Process parameters	Value
Continuous-wave laser power [W]	600
Feed rate [mm·min^{-1}]	450
Track offset [mm]	1
Overlap [%]	50
Powder mass flow rate [g·min^{-1}]	3.3
Shielding gas flow rate [L·min^{-1}]	14

Hardness was measured both superficially and in the cross-sections. Surface measurements were realized at 49 N with an Ernst Compumet SC hardness tester after grinding the deposited part until an average roughness below 1 μm was attained. Micro-hardness measurements along the cross-sections were performed at 2.9 N with a dwell time of 12 s using a micro-Vickers hardness tester, Future-Tech FM-800.

Pin-on-disk tests

In order to investigate the friction and wear behavior of the deposited coatings under sliding conditions, pin-on-disk tests were performed according to the ASTM G99 standard [39] using a Microtest MT pin-ondisk tribometer, shown in Fig. 4.

A tungsten carbide spherical pin with a diameter of 6.0 ± 0.0025 mm supplied by Goodfellow was used for the tests, while the counter surface was made of AISI H13 tool steel. The tests were carried out at room temperature, and the parameters were a load of 20 N, a sliding speed of 0.42 m·s^{-1} and a total distance of 1000 m. The specimens were ground in order to ensure their flatness and obtain an average roughness below 1 μm, the value recommended by the ASTM G99 standard [39]. In each part, six measurements were performed using a Surtronic Duo Surface Roughness Tester from Taylor Hobson, three in the longitudinal grinding direction, Ra_L, and three in the transversal, Ra_T. The obtained results are shown in Table 3.

Prior to testing, and before measuring, the specimen was cleaned with acetone. After cleaning, the wear of the disk and pin was measured

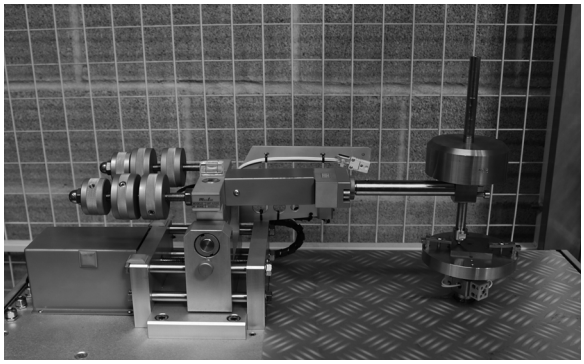

Fig. 4. Microtest MT pin-on-disk tribometer.

Table 3
Arithmetic average in microns of the roughness profile of the specimens before pin-on-disk tests.

Specimen	Ra_{L1}	Ra_{L2}	Ra_{L3}	Ra_{T1}	Ra_{T2}	Ra_{T3}	Ra average
Reference AISI H13 tool	0.14	0.14	0.14	0.18	0.24	0.26	0.18
AISI H13 coating over AISI 1045 substrate	0.14	0.13	0.12	0.20	0.27	0.26	0.19

using a Leica DCM3D confocal microscope. In the present case, both the disk and pin wear were detected. Therefore, the wear suffered by the specimens was measured according to the material loss in the pin and the resulting groove in the surface of the material being tested. In the case of disk wear, the average wear-track profile was measured to obtain the track cross-section area, and multiplied by the average track length to obtain the disk wear volume. In the case of pin wear, the wear scar profile was measured in two orthogonal directions, to obtain the average profile, and compare it with the original profile. In addition, the evolution of the coefficient of friction during the test was also analyzed.

Compression tests

Aiming to investigate the compression resistance of a bimetallic tool made of AISI 1045 and coated with AISI H13, three different coating thicknesses (1, 3, and 5 mm) deposited over a substrate of 200 × 120 × 40 mm^3 were subjected to compression tests. To that end, an Instron 8801 servohydraulic fatigue testing machine was used, whose technical characteristics are detailed in Table 4.

Table 4
Technical characteristics of the Instron 8801 fatigue testing system used.

Feature	Value
Force capacity [kN]	± 100
Stroke [mm]	150
Load weighing accuracy [%]	± 0.002 % of load cell capacity

Table 5
Performed compression tests.

Applied pressure [MPa]	Surface [mm^2]	Applied force [kN]
15	113.1	1.70
30		3.39
45		5.09

To apply the desired pressures on a localized area of each coating thickness, a 12-mmdiameter stainless steel cylinder pin was used. Three different pressures were applied on each coating thickness: one according to the maximum pressure on service for hot stamping tools, 15 MPa, and another two with safety factors of two and three, thus resulting in pressure values of 30 and 45 MPa, respectively. In order to avoid any test interfering with others, each experiment was performed on a different coating. In addition, the velocity employed was 40 mm·s^{-1}, and the total duration of each test was 20 s, emulating hot stamping tools service conditions. The parameters of the tests are shown in Table 5.

After performing the compression tests, the samples were first visually inspected and then analyzed using a Leica DCM3D confocal microscope, so that 3D maps of the areas subjected to the tests were generated.

Thermal modelling of the tools' cooling capacity

3. D model geometry configuration

In order to determine the thermal behavior of bimetallic tools, as well as the required stamping cycle-time to ensure the hardening of the stamped part, a thermal model was developed. Aiming to determine the cooling capacity of the hot stamping tools with an AISI 1045 core and AISI H13 coating, simulations for different coating thicknesses (1, 3, and 5 mm) were performed. An additional simulation for a conventionally manufactured AISI H13 tool set was also performed for further comparison with the coated specimens.

A 3D model comprising the upper tool, the boron steel blank, and the lower tool was developed, as shown in Fig. 5. On the one hand, the total dimensions of the upper and lower tools were 200 × 120 × 40 mm^3, which included an AISI 1045 core and different AISI H13 coating thicknesses (1, 3, or 5 mm) depending on each configuration to be studied. In addition, the tools were actively cooled by water; thus, each tool included six 6-mm-diameter ducts, which were located at 13 mm from the hot surface of the tools, and the distance between consecutive ducts was 20 mm. On the other hand, and according to literature, a thickness of 1.95 mm was selected for the boron steel blank [40,41], which was made of Usibor® 1500 (22MnB5).

Governing equations

The commercial software ANSYS Fluent was employed to perform these simulations. A thermal transient simulation was carried out concerning the fluid-dynamic phenomena inside the cooling ducts. A turbulent flow was considered for the cooling water due to the variations in the velocity and pressure fields in both space and time, so the standard κ-ε model was employed in the simulations. The main transport equations on which the performed simulations were based are summarized below [42]:

$$\frac{\partial}{\partial t}(\rho k) + \frac{\partial}{\partial x_i}(\rho k u_i) = \frac{\partial}{\partial x_j}\left[\left(\mu + \frac{\mu_t}{\sigma_k}\right)\frac{\partial k}{\partial x_j}\right] + G_k + G_b - \rho\varepsilon - Y_M + S_k \quad (2)$$

$$\frac{\partial}{\partial t}(\rho \varepsilon) + \frac{\partial}{\partial x_i}(\rho \varepsilon u_i) = \frac{\partial}{\partial x_j}\left[\left(\mu + \frac{\mu_t}{\sigma_\varepsilon}\right)\frac{\partial \varepsilon}{\partial x_j}\right] + C_{1\varepsilon}\frac{\varepsilon}{k}(G_k + C_{3\varepsilon}G_b) - C_{2\varepsilon}\rho\frac{\varepsilon^2}{k} + S_\varepsilon \quad (3)$$

In Eqs. (2) and (3), G_k represents the generation of turbulence kinetic energy due to the mean velocity gradients, G_b is the generation of turbulence kinetic energy due to buoyancy, and Y_M represents the contribution of the fluctuating dilatation in compressible turbulence due to the overall dissipation rate. Besides, σ_k and σ_ε are the turbulent Prandtl numbers for κ and ε, which are considered with the standard values of 1.0 and 1.3, respectively. $C_{1\varepsilon}$ and $C_{2\varepsilon}$ are user-defined constants, which in the present case, take the values of 1.44 and 1.92, respectively. These values are the default ones proposed by Launder and Spalding [42] and are widely accepted. Finally, S_k and S_ε are user-defined source terms.

From the previous Eqs. (2) and (3) the values of κ and ε can be obtained and, based on them, the turbulent viscosity μ_t is defined according to the following Eq. (4), where the constant C_μ has a value of 0.09.

$$\mu_t = \rho \cdot C_\mu \frac{k^2}{\varepsilon} \quad (4)$$

Material properties

The materials that took part in the present simulations are AISI 1045 mediumcarbon steel, AISI H13 tool steel, Usibor® 1500 boron steel, and water as a coolant of the tools. The default properties for water defined in the ANSYS Fluent materials database and shown in Table 6 were considered suitable. As the temperature difference between the water inlet and outlet was estimated to be below 10 °C [3], water properties were considered constant along the simulated process.

Regarding AISI 1045, AISI H13, and Usibor® 1500, the default properties for steel defined in ANSYS Fluent were initially set. Thermal properties such as the specific heat and thermal conductivity were modified so that they were temperaturedependent, as detailed in Table 7.

Thermal diffusivity of the deposited AISI H13

The employment of thermal conductivity values obtained from the bibliography is an accepted customary practice when modelling the thermal behavior of the hot stamping process. Nevertheless, due to the directional nature of the DED process and the fact that the desired geometry is obtained by overlapping successive clads and layers, the real thermal conductivity of the as-deposited material may differ from that obtained via casting. In fact, it has been reported that thermal conductivity can be decreased by volume defects, such as cracks and porosity, which lower the density of the material. In addition, a high number of dislocations and grain boundaries in the microstructure can also lead to lower thermal diffusivity values [43,44].

Therefore, in order to define the thermal conductivity of the deposited AISI H13 tool steel, the thermal diffusivity was experimentally measured by means of the flash method, which is a well-established technique for measuring the thermal diffusivity of materials [45]. The measurements were performed at different planes situated at 2, 4, and 6 mm from the surface of the substrate. Thermal conductivity, k, and thermal diffusivity, α, are related according to Eq. (5), where ρ and c_p represent the density and specific heat of the material, respectively.

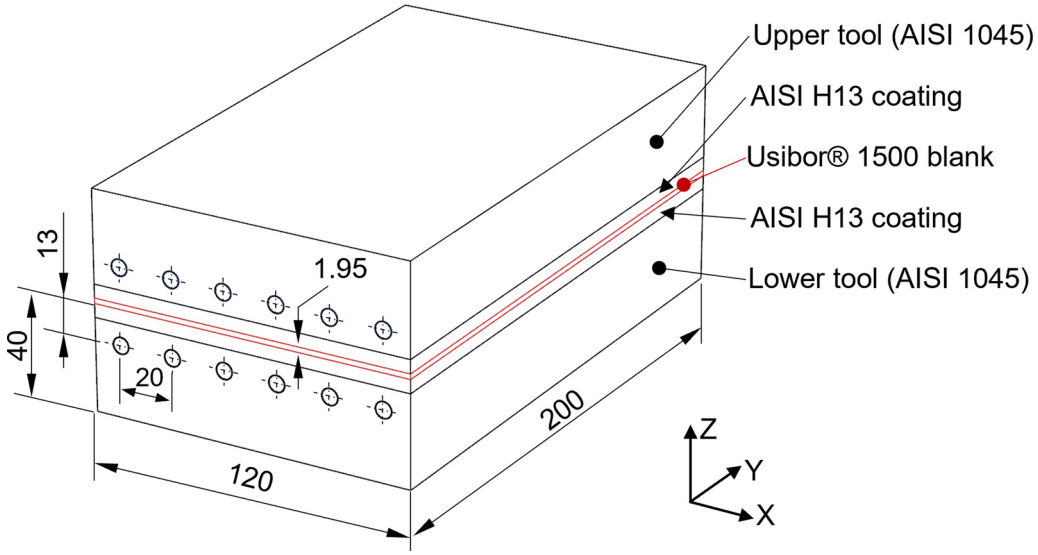

Fig. 5. The 3D model geometry employed.

Table 6
Water properties, data from the ANSYS Fluent database.

Properties	Value
Density [kg·m^{-3}]	998.2
Specific heat [J·kg^{-1}·K^{-1}]	4182
Thermal conductivity [W·m^{-1}·K^{-1}]	0.6
Viscosity [kg·m^{-1}·s^{-1}]	1.003·10^{-3}
Molecular weight [kg·kmol^{-1}]	18.015
Standard enthalpy [J·kmol^{-1}]	−2.858·10^{-8}
Standard entropy [J·K^{-1}·mol^{-1}]	6.990·10^{-4}
Surface tension [N·m^{-1}]	7.194·10^{-2}

$$\alpha = \frac{k}{\rho \cdot c_p} \tag{5}$$

Boundary and initialization conditions

Regarding the cooling water flow, a pressure of 0.3 MPa was defined as a boundary condition for the water inlet into the cooling ducts of the tools. This led to a water velocity in the ducts of above 1 m·s^{-1} so that the Reynolds number was higher than 2300, and a turbulent regime was guaranteed [46,47]. The quenching time of the stamping process was estimated to last 20 s [7]. As far as initialization parameters are concerned, at the beginning of each stamping operation, the water in the cooling ducts was at room temperature (298 K) and the hot blank at 1200 K [40,46–49].

Concerning the temperature of the tools, two sets of initialization parameters were selected to distinguish between the hot stamping of the first blank and the following one, and thus adjust it to actual production circumstances. In this way, the stamping tools were considered to be at room temperature (298 K) before stamping the first blank, whereas their temperature was increased until 348 K (75 °C) [40] to simulate a stable-regime hot stamping process.

Results and discussion

Material characteristics

First, the feasibility of depositing AISI H13 metallic powder over an AISI 1045 substrate needed to be approached. To that end, a metallographic analysis was performed, and the results of such analysis are presented below:

In Fig. 6, a detail of a crosssection is shown. The lighter upper zone is the melted area during the deposition of the top layer. In details 1 and 2, the bonding between adjacent layers is shown. As can be witnessed, neither cracks nor lack-of-fusion regions were detected. In detail 3, the microstructure of a central region in a clad is shown, where columnar dendrites can be seen. The dendrites grow along the direction of higher temperature gradient, usually perpendicular to the clad boundary, which is in line with previous work conducted by other researchers [49]. Last, in detail 4, the transition between the AISI 1045 substrate and the deposited AISI H13 is shown. The zone affected by the additive process is minimal, and good penetration is ensured, which guarantees a sound metallurgical bonding. The microstructure of the base material remains unaffected after the DED process.

After that, in the second step, the five crosssections extracted were analyzed. In each case, an area of 5 × 8 mm^2 was studied by means of the Image Processing Toolbox from the Matlab 2018b software, so that both the percentage and size of the pores in the region of the deposited material could be determined. Each pixel corresponded to a 12.5 × 12.5 μm^2 area, which determined the minimum size of the pores that

Table 7
Thermal properties employed [36,37,40].

Material	Thermal properties	Temperature [K]					
		293	473	673	873	1073	1273
AISI 1045	Specific heat [J·kg^{-1}·K^{-1}]	475	495	565	700	700	700
	Thermal conductivity [W·m^{-1}·K^{-1}]	47.6	40.4	36.2	32.0	32.0	32.0
AISI H13	Specific heat [J·kg^{-1}·K^{-1}]	461	475	519	592	592	592
	Thermal conductivity [W·m^{-1}·K^{-1}]	24.9	27.4	29.1	28.5	28.5	28.5
Usibor® 1500	Specific heat [J·kg^{-1}·K^{-1}]	444	520	563	581	590	603
	Thermal conductivity [W·m^{-1}·K^{-1}]	30.7	30.0	21.7	23.6	25.6	27.6

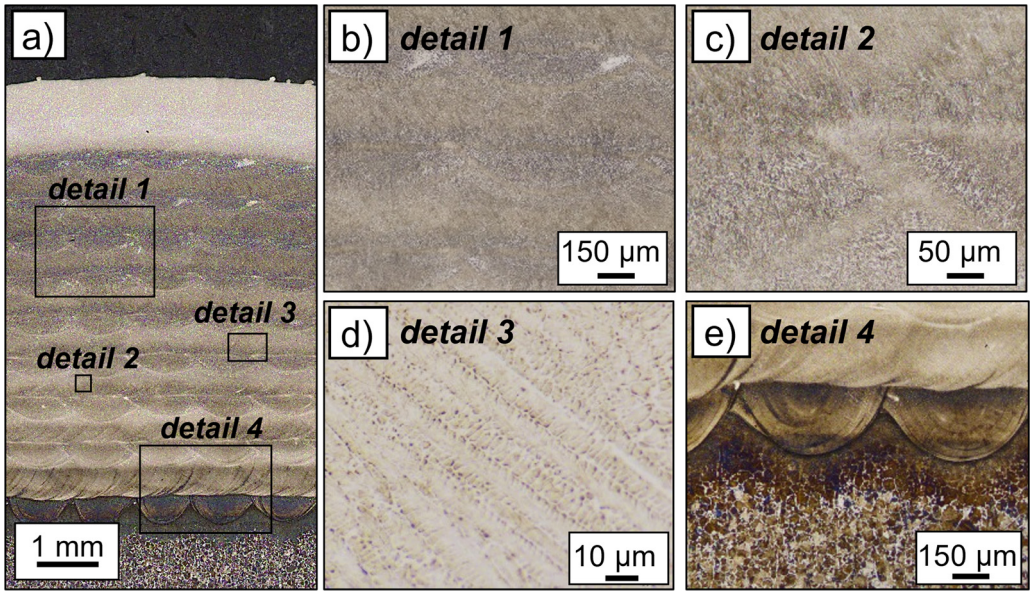

Fig. 6. Metallographic analysis of the tests.

the software could detect.

An example of the post-processed image of a crosssection is presented in Fig. 7a, where the areas with material are displayed in white, and those with no material are represented in black. Additionally, micrographs of pores of different sizes are detailed in Fig. 7b and c. Last, the collected results are included in the graph shown in Fig. 7d, which represents the pore size distribution with regard to the total porosity measured. Despite single porosity values being measured, they are connected with straight lines in order to make the obtained results more illustrative. In this way, blue lines correspond to the five crosssections analyzed, and the red one is the average value. In all cases, the pore size remained below 150 µm in diameter.

The total porosity and pore-size distribution values measured in each crosssection are detailed in Table 8. An average total porosity of 0.219 % was obtained, which means that the deposited material was more than 99.5 % dense. In terms of pore size distribution, in all cases, the pores detected had a diameter of less than 150 µm and, on average, 83.2 % of the pores had a diameter of less than 100 µm and the 14.4 % of less than 25 µm.

The metallographic analysis manifested a high-quality deposition of the AISI H13 tool steel over AISI 1045, free of cracks. The bonding between both the deposited material and the substrate, and that between adjacent deposited layers was sound. Besides, no lacks of fusion were detected. In terms of porosity, the deposited material was found over 99.5 % dense, with pores below 150 µm in diameter.

Thus, the metallurgical quality of the deposited material was good,

Table 8
Porosity analysis results.

Test	Total porosity [%]	Pore diameter distribution [%] as a function of the total porosity			
		< 25 µm	< 100 µm	< 150 µm	< 200 µm
1	0.213	9.3	100.0	100.0	100.0
2	0.258	18.5	72.8	100.0	100.0
3	0.252	23.1	100.0	100.0	100.0
4	0.183	9.8	60.3	100.0	100.0
5	0.192	11.5	82.8	100.0	100.0
Average	0.219	14.4	83.2	100.0	100.0

and the compatibility between the materials employed demonstrated satisfactory results. Therefore, the suitability of combining AISI H13 and AISI 1045 in the same part is demonstrated.

Mechanical behavior

Hardness tests

Hardness was measured both superficially and indepth across the deposited layers. On the one hand, average hardness values of 56.5, 53.8, and 53.2 HRC were measured for the surfaces of 1, 3, and 5 mm thick coatings deposited, respectively. In all cases, attained hardness was higher than 50 HRC, which was the minimum hardness value required in hot stamping applications. Additional measurements were

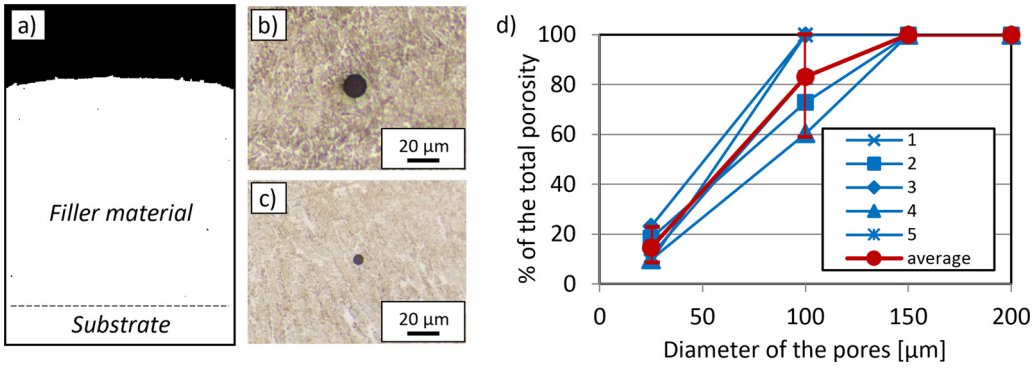

Fig. 7. (a) Post-processed image of a cross-section; (b), (c) details of pores; (d) Total porosity as a function of pore size.

Table 9
Hardness values for the different coating thicknesses.

Test	Hardness [HRC]			
	Cast AISI H13	Coating thickness		
		1 mm	3 mm	5 mm
1	56.0	59.1	54.1	53.2
2	55.6	55.6	52.9	52.7
3	54.9	54.7	53.1	53.2
4	55.6	56.5	54.2	52.1
5	55.6	57.0	55.9	52.9
6	56.7	57.4	51.8	54.0
7	56.2	55.8	54.1	53.6
8	56.4	55.8	54.0	53.9
9	56.9	54.8	54.9	53.6
10	55.8	58.3	53.1	52.6
Average	56.0	56.5	53.8	53.2

also performed on the cast AISI H13, resulting in an average hardness value of 56.0 HRC. These average values were calculated after ten measurements, as shown in Table 9.

On the other hand, microhardness measurements were performed on four cross-sections of a 7 mm thick AISI H13 deposition. The values across the different layers of material are shown in Fig. 8. In all sections analyzed, the deposited material presented a constant hardness higher than 55 HRC across its different layers. On the contrary, this value decreased until 20–25 HRC when the AISI 1045 substrate was reached. This was expected, as the hardness of AISI 1045 medium-carbon steel is reported to be 220–250 HV [36].

Given the results, and considering the field of application of the present work, the hardness and micro-hardness values obtained were satisfactory in terms of the materials and technology employed. In addition, there was no need for additional heat treatment to attain the high hardness required in hot stamping tools. Moreover, hardness results maintained uniform values on the different surfaces and sections analyzed.

Friction and wear tests

A pin-ondisk tribometer was used to characterize the AISI H13 coating deposited on an AISI 1045 substrate and compare it with a reference AISI H13 tool. The results of the laser deposited AISI H13 coating case are shown in Fig. 9, in which the wear of both the coating and the pin employed are shown.

Wear scar measurement was done in four representative locations of the disk surface, which were separated 90°. In each case, the 3D map of the surface was obtained by measuring multiple profiles, and the average profile was extracted as an average of 60 profiles. In each case, the width, depth, and area of the groove were measured using the surface imaging and the Leica Map metrology software. Values shown in Table 10 represent the average of the four individual measurements. In the case of pin wear, the profile of the wear scar was directly extracted from the 3D map, and average values were obtained, which are also detailed in Table 10. As can be noticed, the wear volume in both the specimen and the pin was slightly lower in the case of the laser-deposited AISI H13 coating.

The friction signals recorded during the wear test are shown in Fig. 10. The signals present an initial metal-metal contact before stabilizing upon the formation of an interfacial layer on the pin surface due to the transfer of material from the disk, consisting of metal and oxide debris. In this way, the friction coefficient was first increased to the maximum value due to the static frictional force and then decreased in the stable stage. In comparison, the laser-deposited AISI H13 coating presented a longer starting stage (about 190 m) and a slightly lower maximum friction coefficient value (0.70) than the reference AISI H13 tool, which presented approximate values of 75 m and 0.75, respectively. After this stage, the friction coefficient of DED and the reference AISI H13 was lowered to average values of 0.57 and 0.55, respectively. Nevertheless, the final value for the DED AISI H13 coating after 1000 m travelled distance was 0.61, which was slightly higher than that of the cast AISI H13 (0.58). In addition, the DED AISI H13 signal showed more significant fluctuations than the reference AISI H13 test, which was attributed to the adhesive wear mechanism.

Therefore, it can be concluded that the friction and wear behavior of

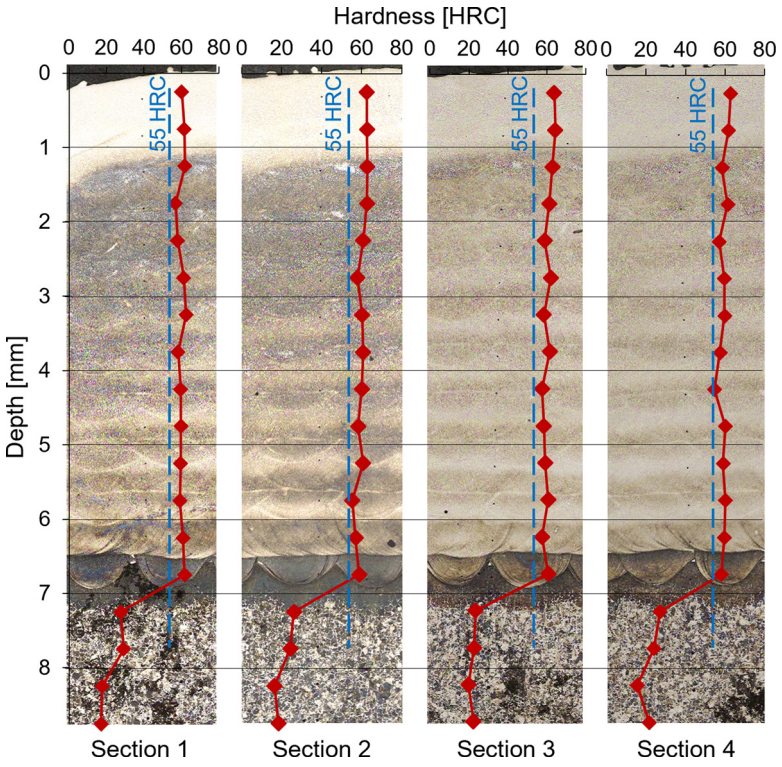

Fig. 8. Hardness values of the deposited material and substrate.

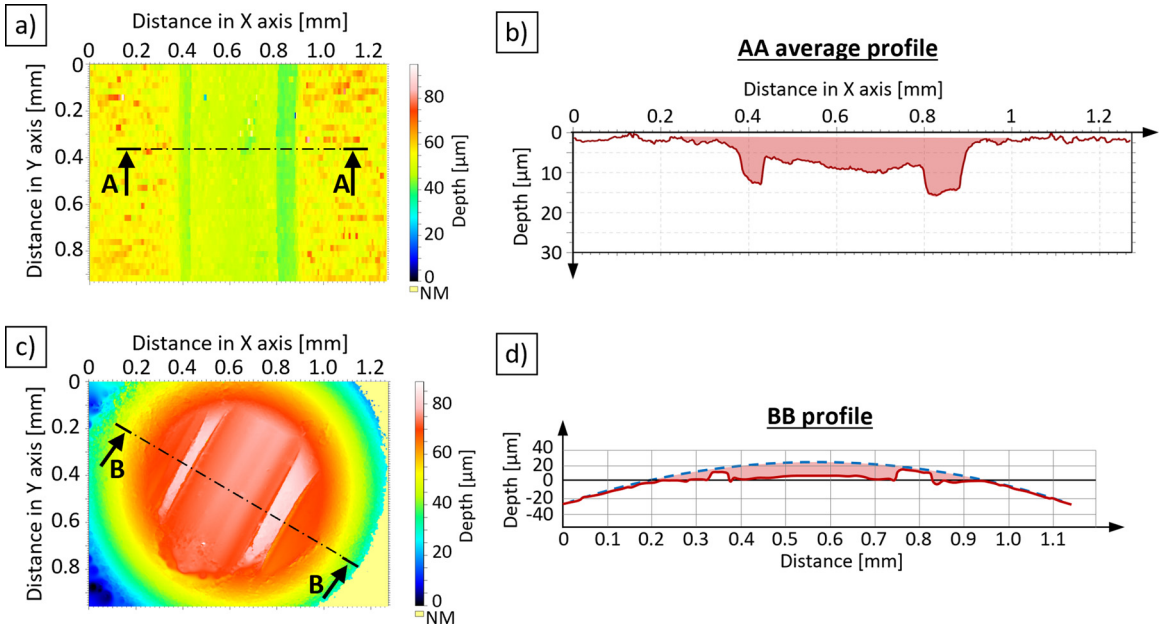

Fig. 9. Results of the pin-on-disk tests for the (a), (b) AISI H13 coating and (c), (d) spherical pin.

Table 10
The pin-on-disk test results.

	Conventional AISI H13 tool	1 mm AISI H13 coating over AISI 1045 substrate
Specimen wear		
Wear width [mm]	0.532	0.537
Wear depth [mm]	0.015	0.014
Area [mm^2]	$4.359 \cdot 10^{-3}$	$4.005 \cdot 10^{-3}$
Track radius [mm]	15	15
Wear volume [mm^3]	0.411	0.377
Pin wear		
Wear diameter [mm]	0.692	0.656
Pin diameter [mm]	6	6
Wear depth [mm]	0.018	0.017
Wear volume [mm^3]	0.256	0.240

the laser-deposited AISI H13 tool steel, and the AISI H13 reference were comparable.

Compression tests

Considering the severe service conditions stamping tools are subjected to during their operating life, a mechanical validation test in terms of compression was performed. Coatings 1, 3, and 5 mm thick deposited via DED were tested and compared with the cast material. Results are presented in several graphs, where the evolution of the applied force as a function of both time and displacement on the executed tests is shown (see Fig. 11).

On the one hand and attending to the graph where force is represented as a function of time, the three coatings tested presented the same trend. In fact, two stages can be distinguished: first, a transient stage, where the applied force is increased until the set point value (1.70, 3.39 and 5.09 kN for 15, 30 and 45 MPa, respectively) is reached; second, a stationary stage, where the applied force is kept constant around the set point value until the test is concluded.

On the other hand, when analyzing the graph where the force is represented as a function of displacement, other observations can be made. For each force value applied, each thickness behaves differently; that is, the thinner the coating, the lower is the displacement suffered to attain the desired force. In addition, each tested thickness presents a similar slope, regardless of the force applied.

In order to represent the behavior of bimetallic tools made of AISI 1045 and coated with AISI H13 versus conventional AISI H13 tools, a comparison of their performance at 30 MPa is shown in Fig. 12a. On the one hand, 1 and 3 mm coatings behaved similarly to the reference tool, which proves the suitability of bimetallic tools in these terms. On the other hand, the 5 mm coating presented a slightly higher deformation. Nevertheless, and after analyzing all the tested surfaces, both visually and by means of the 3D-mapping with a Leica DCM3D confocal

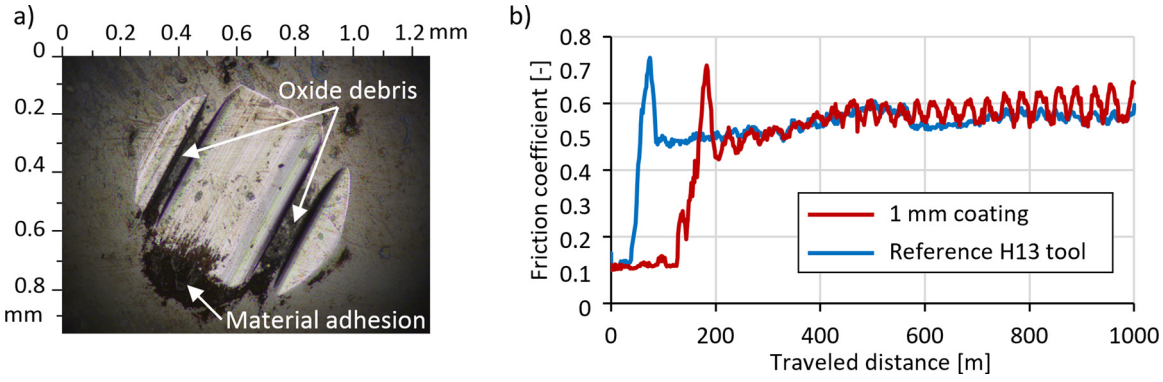

Fig. 10. (a) The worn surface of the pin; (b) Friction coefficient results.

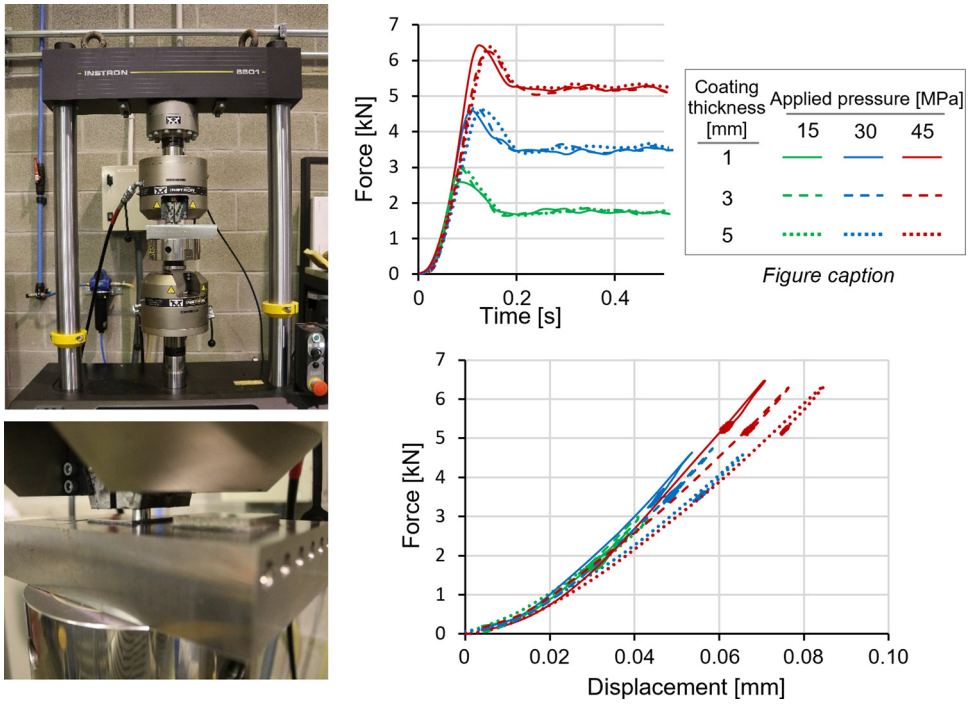

Fig. 11. Set-up (left) and results (right) of the compression tests.

microscope, no changes or damage were detected in any specimen. In order to illustrate this matter, a 3D map of the 3 mm thick coating tested under 30 MPa pressure is included in Fig. 12b.

Therefore, it is concluded that bimetallic tools coated via DED withstand more than three times the service pressure required in hot stamping processes, which was set at 15 MPa. Nevertheless, obtained results depend on the deposited thickness, so that the best performance in terms of equivalency with the reference tool was attained with 1 and 3 mm thick coatings.

Thermal model results

Experimental thermal conductivity measurement of the deposited AISI H13

The experimental thermal diffusivity value of the deposited AISI H13 was measured by means of the flash method at 20 °C, attaining an average value of 5.72 $mm^2 \cdot s^{-1}$. This value was slightly lower than that provided by manufacturers. The main reasons for this are the microstructure and different grain solidifying directions developed within the deposited material. These grain boundaries work as thermal barriers, thus reducing thermal diffusivity.

Based on the experimental measurement of the diffusivity manifested and using Eq. (5), the thermal conductivity value for the deposited AISI H13 tool steel was calculated, which resulted in 20.70 $W \cdot m^{-2} K^{-1}$. Since this value is 16.87 % lower than the parameter of the cast AISI H13 at 20 °C supplied by manufacturers and considered in Table 7, the thermal conductivity of AISI H13 deposited via DED was subsequently modified in the simulations. In this way, the corrected thermal conductivity value for the deposited AISI H13 was 83.13 % of the values supplied for the cast AISI H13. Thermal conductivity values used in the simulations are detailed in Table 11.

Cycle-time reduction

Two different thermal situations were simulated: on the one hand, the stamping tools were considered at room temperature (298 K) before stamping the first blank; on the other hand, a stable hot stamping process situation where the tools were initially at 348 K (75 °C). The results analysis is focused on the case where the tools were initially at 348 K (75 °C), as these are considered more restrictive and

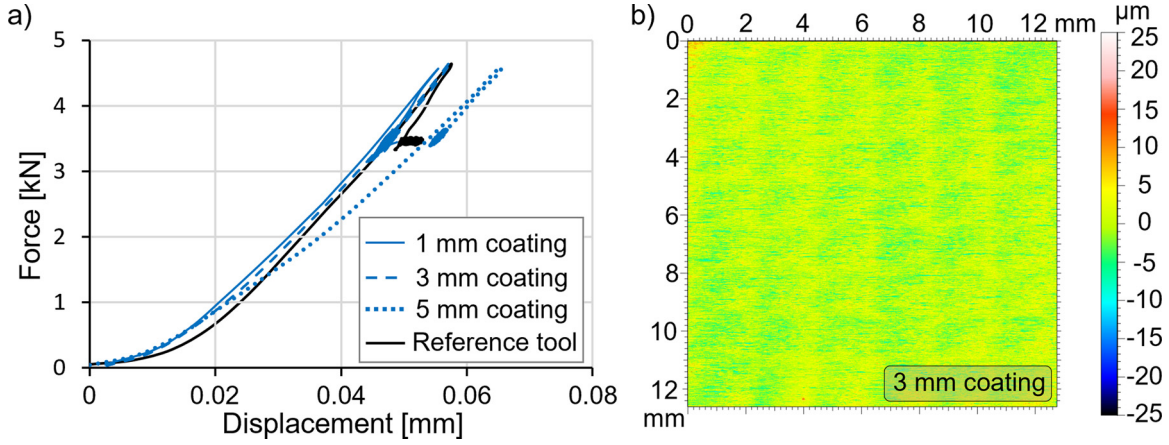

Fig. 12. (a) Comparison with the reference tool; (b) 3D map of the 3 mm coating tested at 30 MPa.

Table 11
Experimentally determined thermal conductivity of the DED deposited AISI H13.

Material	Property	Temperature [K]					
		293	473	673	873	1073	1273
Deposited AISI H13	Thermal conductivity [$W \cdot m^{-1} \cdot K^{-1}$]	20.7	22.8	24.2	23.7	23.7	23.7

representative of long working situations. In Fig. 13, the maximum temperature of the blank during the cooling stage is shown for the different configurations simulated in the present case.

On the one hand, when conventional AISI H13 tools are considered, the temperature of the blank at the end of the stamping operation, that is, after 20 s of simulation, was 341 K (68 °C). On the other hand, tools composed of an AISI 1045 core and coated with AISI H13 reached the same temperature in a shorter time, thus reducing the time required for each stamping operation. These cycletime reductions were quantified for each case, and results are shown in Table 12. The thinner the deposited coating, the higher the time reduction experienced, enabling a cycle-time reduction of up to 44.5 % when a 1 mm thick AISI H13 coating is considered. This was actually expected because the thermal conductivity of AISI 1045 is significantly higher than that of AISI H13.

Another critical point when guaranteeing homogeneous properties in the final part is the temperature distribution in the surface of the tools, as it is directly translated into unequal cooling. This may result in an unsuccessful quenching of the stamped part, thus leading to undesired material microstructures and negatively affecting its mechanical properties. To analyze the temperature distributions of the tools-blank set, the thermal profile of the contact surface between the tool and the blank in the middle plane was extracted. Temperature distributions and results at a time instant t = 2 s attained for each geometry simulated are shown in Fig. 14.

The maximum, minimum, and mean temperatures were extracted for each case and detailed in Table 13. Lower coating thicknesses led to lower mean temperatures on the surface of the tools. This is due to the higher thermal conductivity of the AISI 1045 used as core material in these cases. Besides, it must be accounted for that a lower coating thickness also led to higher temperature variations on the surface because of higher thermal conductivity. Nevertheless, in the present case,

Table 12
Cycle-time reduction.

	Conventional AISI H13 tool	Coating thickness		
		5 mm	3 mm	1 mm
Time instant [s] when T = 341 K	20.0	12.8	11.7	11.1
Time reduction [s]	-	7.2	8.3	8.9
Cycle-time reduction [%]	-	36.0	41.5	44.5

temperature variations were kept below minimum values, 3 K, and therefore, their influence on the process can be neglected.

In Fig. 15, a comparison between the thermal fields in the middle plane of the tools is presented. The three images were obtained at a 20 s time instant from the beginning of the cooling process, which corresponded to the end of the quenching time of the stamping process. As can be seen from the figure, heat dissipation from the blank was higher for the 1 mm thick coating.

Hence, by coating AISI 1045 mild steel cores with the AISI H13 tool steel, an enhanced thermal performance was obtained. In this way, an improvement was attained in the stamping process, both in terms of cycle-time reduction and temperature reduction.

Discussion on the cooling capability of the additively manufactured bimetallic tools

After the analysis of the results in section *5.1 Material characteristics*, it can be concluded that the deposited material is almost fully dense, with a density above 99.5 %, and free of internal defects. Therefore, the main reasons for the experimentally measured 16.87 % lower thermal conductivity of the DED AISI H13 than that of the cast AISI H13 are the thinner microstructure and the different grain solidifying directions developed as a consequence of the fast cooling rates achieved in the DED process.

Subsequently, if the hot stamping tools are to be fully manufactured via DED, this phenomenon will reduce considerably the heat transfer capability of the tools, including lower IHTC and CHTC coefficients.

Nevertheless, if an AISI 1045 tool core is employed and just the outer AISI H13 coating is manufactured via DED, the effect of this lower thermal conductivity of the DED AISI H13 is minimized and the total

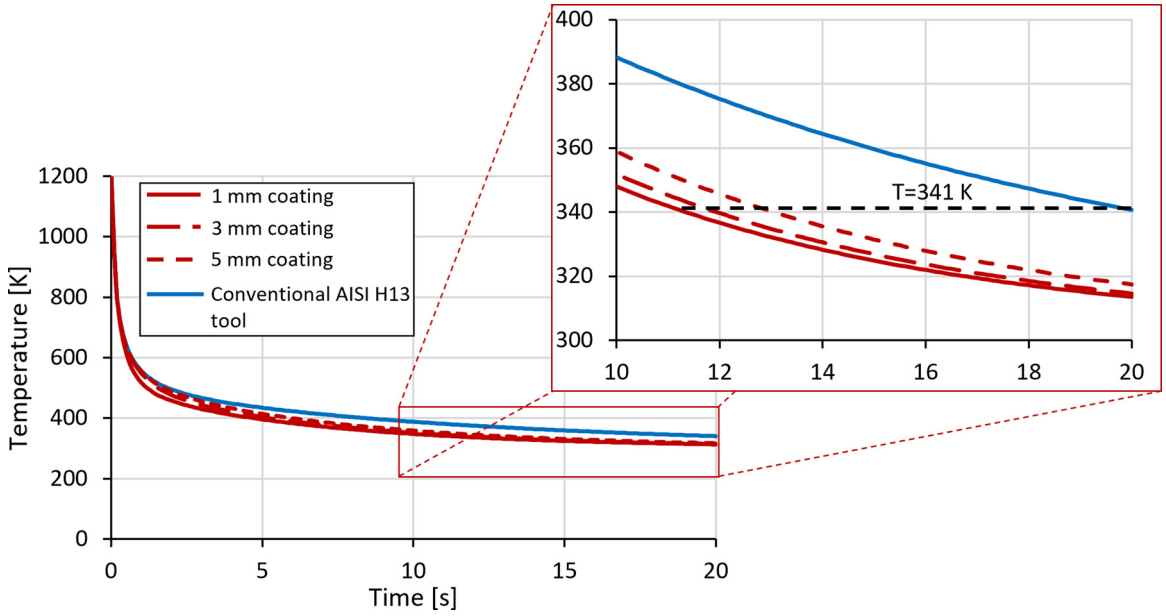

Fig. 13. Maximum temperature of the blank (left); detail of the cycle-time reduction (right).

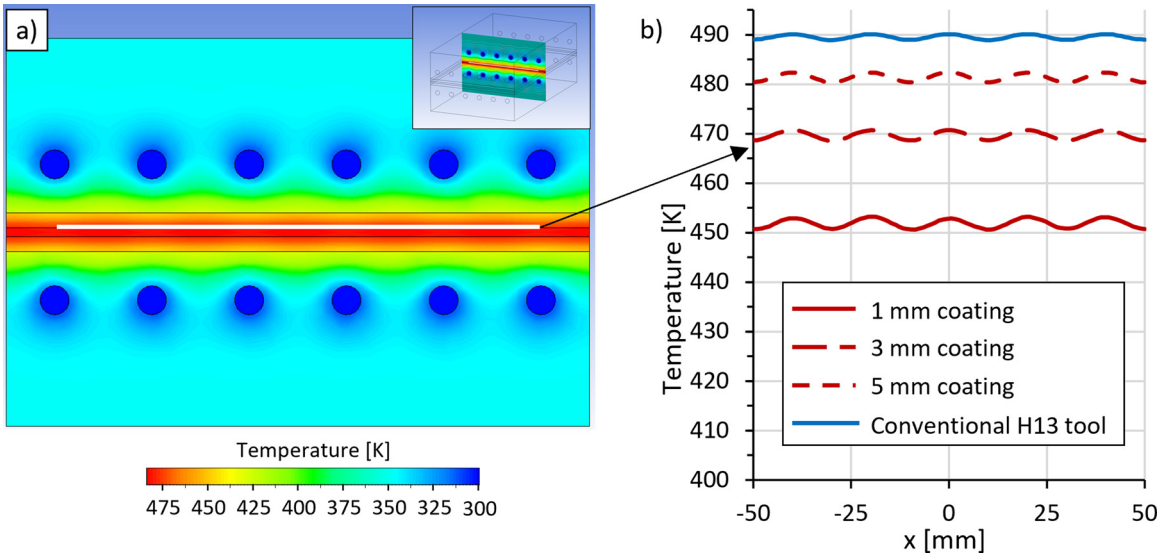

Fig. 14. (a) Temperature distribution in the middle plane of the tool at t = 2 s (3-mm-thick AISI H13 coating); (b) Temperature profile in the tool-blank interface at t = 2 s.

Table 13
Temperature evaluation results in the surface of the tools at t = 2 s.

	Conventional AISI H13 tool	Coating thickness		
		5 mm	3 mm	1 mm
Maximum temperature [K]	490.09	482.37	470.73	453.24
Minimum temperature [K]	488.89	480.35	468.54	450.60
Mean temperature [K]	489.49	481.36	469.64	451.92
Temperature variation [K]	1.21	2.02	2.19	2.64

effective conductivity of the tool improves that of the conventional AISI H13 tool. In particular, for the present case study, the stamping cycle-time is reduced up to 44.5 %.

Conclusions

In the present work, an investigation on bimetallic hot stamping tools manufactured via laser-based DED has been performed. To that end, the suitability and advantages of this novel approach have been studied, both in terms of manufacturability and performance, and in comparison with conventionally manufactured tools. Based on the results obtained, the following conclusions were drawn:

- The feasibility of depositing the AISI H13 tool steel over the AISI 1045 steel and their subsequent metallurgical compatibility was demonstrated. Dilution, porosity, and microstructure were investigated for the material characteristics of the deposited AISI H13. As a result, no cracks were found either in the deposited material or in the interface between AISI H13 and AISI 1045. In addition, obtained porosity within the deposited material was kept below 0.5 %, while the average diameter of the pores was lower than 150 μm. Therefore, the quality of both the deposited material and bonding

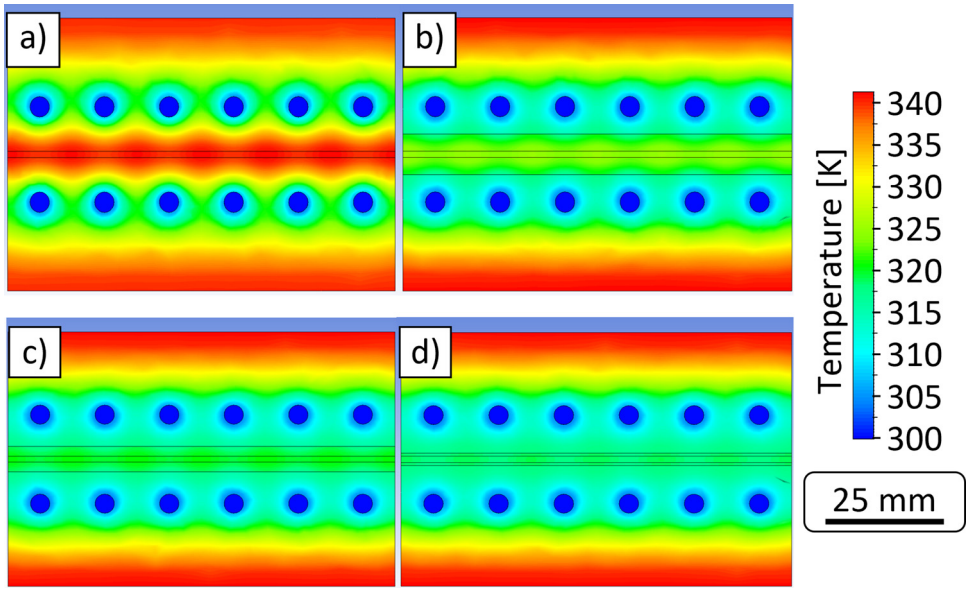

Fig. 15. Temperature distribution in the middle plane of the tool at t = 20 s for (a) conventional tool; (b) 5 mm; (c) 3 mm; and (d) 1 mm AISI H13 coating.

with the substrate were guaranteed.

- Regarding mechanical properties, the laser-deposited AISI H13 presented similar characteristics to those of the cast AISI H13. As far as friction and wear are concerned, a friction coefficient variation of 0.03 was obtained between both materials, while the wear volume values were found similar. Hence, comparable friction and wear behavior was concluded. Hardness measurements show that the deposited material presented a uniform hardness distribution with a minimal variation and a similar surface value as the cast AISI H13. Slightly higher values were obtained when thin coatings were deposited. Finally, with regard to the compression tests, both materials were found to present behavior similar to that of the reference AISI H13 tool. Nevertheless, results obtained with 1 and 3 mm thick coatings adjusted better to the reference.
- In order to obtain reliable results in thermal simulations that involve additively manufactured parts, the real thermal conductivity of the deposited material must be considered, which is lower than the values provided in literature. In the present case, the actual thermal conductivity value for laser deposited AISI H13 was 83.13 % of the values supplied for the cast AISI H13.
- Finally, the production rate increase that bimetallic tools developed by DED offer when compared to conventional tools was determined via thermal simulations. Maximum cycle-time reductions were obtained when an AISI 1045 core was combined with a minimum AISI H13 coating thickness. In the present case and for the studied geometry, AISI 1045 tools coated with 1 mm AISI H13 reduced cycle time by 44.5 % compared with the cast H13.

Hence, this work demonstrates the feasibility of manufacturing bimetallic tools by coating a high thermal conductivity mild-steel core with hot work tool steel. Moreover, this approach offers a potential alternative to replace conventional tool steel dies in terms of both thermal behavior and mechanical characteristics. As a result, cost-effective tools with enhanced thermal properties can be attained.

Declaration of Competing Interest

The authors report no declarations of interest.

Acknowledgments

The authors gratefully acknowledge the financial support for this study from the European Union, through the H2020-FoF132016 PARADDISE project (contract number 723440) and from the Spanish Ministry of Economy and Competitiveness for the support on the DPI2016-79889-R INTEGRADDI project.

References

[1] Steinbeiss H, So H, Michelitsch T, Hoffmann H. Method for optimizing the cooling design of hot stamping tools. Prod Eng 2007;1:149–55. https://doi.org/10.1007/s11740-007-0010-3.
[2] Belingardi G, Beyene AT, Koricho EG, Martorana B. Alternative lightweight materials and component manufacturing technologies for vehicle frontal bumper beam. Compos Struct 2015;120:483–95. https://doi.org/10.1016/j.compstruct.2014.10.007.
[3] Lorenz D. Hot Stamping Process Simulation with LS-DYNA Capabilities and Benefits. 2012https://www.dynamore.de/en/downloads/infodays/dokumente/kalt-und-warmumformprozesse2012/hot-stamping-process/view.
[4] Eriksson M, Oldenburg M, Somani M, Karjalainen LP. Test and evaluation of material data for analysis of forming and hardening of boron steel components. Model Simul Mater Sci Eng 2002;10:277–94. https://doi.org/10.1088/0965-0393/10/3/303.
[5] Chang Y, Meng Z, Ying L, Li X, Ma N, Hu P. Influence of hot press forming techniques on properties of vehicle high strength steels. J Iron Steel Res Int 2011;18:59–63. https://doi.org/10.1016/S1006-706X(11)60066-6.
[6] Ganapathy M, Li N, Li J, Bhattacharjee ND. Investigation of a new hot stamping process with improved formability and productivity. Procedia Eng. Elsevier; 2017. p. 771–6. https://doi.org/10.1016/j.proeng.2017.10.827.
[7] Naganathan A, Penter L. Sheet Metal Forming—Processes and Applications Hot Stamping. 2012www.asminternational.org.
[8] Muvunzi R, Dimitrov DM, Matope S, Harms TM. Development of a model for predicting cycle time in hot stamping. Procedia Manuf 2018;21:84–91. https://doi.org/10.1016/j.promfg.2018.02.098.
[9] Chen J, Li X, Han X. Hot stamping. Compr Mater Process 2014;5:351–70. https://doi.org/10.1016/B978-0-08-096532-1.00526-4.
[10] Çengel YA. Chapter 8: Internal Forced Convection. Heat and Mass Transfer. 2007. p. 419–40.
[11] Ghiotti A, Bruschi S, Medea F, Hamasaiid A. Tribological behavior of high thermal conductivity steels for hot stamping tools. Tribol Int 2016;97:412–22. https://doi.org/10.1016/j.triboint.2016.01.024.
[12] Cortina M, Arrizubieta JI, Calleja A, Ukar E, Alberdi A. Case study to illustrate the potential of conformal cooling channels for hot stamping dies manufactured using hybrid process of Laser Metal Deposition (LMD) and milling. Metals (Basel) 2018;8:102. https://doi.org/10.3390/met8020102.
[13] He B, Ying L, Li X, Hu P. Optimal design of longitudinal conformal cooling channels in hot stamping tools. Appl Therm Eng 2016;106:1176–89. https://doi.org/10.1016/j.applthermaleng.2016.06.113.
[14] Valls I, Casas B, Rodríguez N, Paar U. Benefits from using high thermal conductivity tool steels in the hot forming of steels. Metall Ital 2010;102:23–8.
[15] Valls I, Hamasaiid A, Padré A. High thermal conductivity and high wear resistance tool steels for cost-effective hot stamping tools. J Phys Conf Ser 2017;896. https://doi.org/10.1088/1742-6596/896/1/012046.
[16] Chang Y, Hu P, Zhao K, Wu Y, Tang X. Investigation of the factors influencing the interfacial heat transfer coefficient in hot stamping. J Mater Process Technol 2016;228:25–33. https://doi.org/10.1016/j.jmatprotec.2014.10.008.
[17] Cottam R, Wang J, Luzin V. Characterization of microstructure and residual stress in a 3D H13 tool steel component produced by additive manufacturing. J Mater Res 2014;29:1978–86. https://doi.org/10.1557/jmr.2014.190.
[18] Wang SH, Chen JY, Xue L. A study of the abrasive wear behaviour of laser-clad tool steel coatings. Surf Coatings Technol 2006;200:3446–58. https://doi.org/10.1016/j.surfcoat.2004.10.125.
[19] Toyserkani E, Khajepour A, Corbin SF. Laser Cladding. Boca Raton: CRC Press; 2004. https://doi.org/10.1201/9781420039177.
[20] Terrassa KL, Haley JC, MacDonald BE, Schoenung JM. Reuse of powder feedstock for Directed Energy Deposition. Powder Technol 2018;338:819–29. https://doi.org/10.1016/j.powtec.2018.07.065.
[21] Wissenbach K, Treatment Surface. Poprawe R, editor. Tailored Light 2 Laser Appl. Technol. Berlin Heidelberg, Berlin, Heidelberg: Springer; 2011. p. 173–239. https://doi.org/10.1007/978-3-642-01237-2_11.
[22] Gibson I, Rosen D, Stucker B. Directed Energy Deposition Processes. Addit. Manuf. Technol.. New York, New York, NY: Springer; 2015. p. 245–68. https://doi.org/10.1007/978-1-4939-2113-3_10.
[23] Arrizubieta JI, Ruiz JE, Cortina M, Ukar E, Lamikiz A. Evaluacion de la sobreacumulacion de material en los cambios de direccion durante el proceso de aporte. Rev Iberoam Ing Mecánica 2018;22:3–12.
[24] Cortina M, Arrizubieta JI, Ruiz JE, Ukar E, Lamikiz A. Análisis de la influencia del uso de fluido de corte en procesos híbridos de mecanizado y aporte por láser. Rev Iberoam Ing Mecánica 2018;22:33–9.
[25] Bi G, Sun CN, Gasser A. Study on influential factors for process monitoring and control in laser aided additive manufacturing. J Mater Process Technol 2013;213:463–8. https://doi.org/10.1016/j.jmatprotec.2012.10.006.
[26] Ruiz JE, González H, Cortina M, Arrizubieta JI, Lamikiz A. Desarrollo de estrategia Y sensorización en proceso de LMD para reparación de Geometrías tipo blisk. Rev Iberoam Ing Mecánica 2018;22:13–8.
[27] Jeng JY, Lin MC. Mold fabrication and modification using hybrid processes of selective laser cladding and milling. J Mater Process Technol 2001;110:98–103. https://doi.org/10.1016/S0924-0136(00)00850-5.
[28] Imran MK, Masood SH, Brandt M. Bimetallic dies with direct metal-deposited steel on Moldmax for high-pressure die casting application. Int J Adv Manuf Technol 2011;52:855–63. https://doi.org/10.1007/s00170-010-2783-3.
[29] Muro M, Artola G, Gorriño A, Angulo C. Effect of the martensitic transformation on the stamping force and cycle time of hot stamping parts. Metals (Basel) 2018;8:385. https://doi.org/10.3390/met8060385.
[30] Muro M, Artola G, Gorriño A, Angulo C. Wear and friction evaluation of different tool steels for hot stamping. Adv Mater Sci Eng 2018;2018:1–11. https://doi.org/10.1155/2018/3296398.
[31] Hu YP, Chen CW, Mukherjee K. Development of a new laser cladding process for manufacturing cutting and stamping dies. J Mater Sci 1998;33:1287–92. https://doi.org/10.1023/A:1004346214050.
[32] Ocelík V, De Oliveira U, De Hosson JTM. Thick tool steel coatings with laser cladding. WIT Trans Eng Sci 2007;55:13–22. https://doi.org/10.2495/SECM070021.
[33] Navas C, Conde A, Fernández BJ, Zubiri F, de Damborenea J. Laser coatings to improve wear resistance of mould steel. Surf Coatings Technol 2005;194:136–42. https://doi.org/10.1016/j.surfcoat.2004.05.002.
[34] Kattire P, Paul S, Singh R, Yan W. Experimental characterization of laser cladding of CPM 9V on H13 tool steel for die repair applications. J Manuf Process 2015;20:492–9. https://doi.org/10.1016/j.jmapro.2015.06.018.
[35] Patra Karmakar D, Gopinath M, Nath AK. Effect of tempering on laser remelted AISI H13 tool steel. Surf Coatings Technol 2019;361:136–49. https://doi.org/10.1016/j.surfcoat.2019.01.022.
[36] Gao K, Qin X, Wang Z, Chen H, Zhu S, Liu Y, et al. Numerical and experimental analysis of 3D spot induction hardening of AISI 1045 steel. J Mater Process Technol 2014;214:2425–33. https://doi.org/10.1016/j.jmatprotec.2014.05.010.
[37] Oh S, Ki H. Deep learning model for predicting hardness distribution in laser heat

treatment of AISI H13 tool steel. Appl Therm Eng 2019;153:583–95. https://doi.org/10.1016/j.applthermaleng.2019.01.050.
[38] Arrizubieta JI, Tabernero I, Ruiz JE, Lamikiz A, Martinez S, Ukar E. Continuous coaxial nozzle design for LMD based on numerical simulation. Phys. Procedia. Elsevier; 2014. p. 429–38. https://doi.org/10.1016/j.phpro.2014.08.146.
[39] American Society for Testing and Materials, ASTM G99-17: standard test method for wear testing with a pin-on-disk apparatus. Annu B ASTM Stand 2017:1–6. https://doi.org/10.1520/G0099-17.Copyright.
[40] Shapiro AB. Using LS-Dyna for Hot Stamping. 7th Eur. LS-DYNA Conf. 2009:9. https://doi.org/10.1557/PROC-133-269.
[41] Karbasian H, Tekkaya AE. A review on hot stamping. J Mater Process Technol 2010;210:2103–18. https://doi.org/10.1016/j.jmatprotec.2010.07.019.
[42] Launder BE, Spalding DB. Lectures in Mathematical Models of Turbulence. 1972 https://scholar.google.com/scholar_lookup?title=Lectures in mathematical models of turbulence&author=B.E. Launder&publication_year=1972(Accessed 29 April 2019).
[43] Zhang X, Yan Q, Lang S, Xia M, Ge C. Texture evolution and basic thermal-mechanical properties of pure tungsten under various rolling reductions. J Nucl Mater 2016;468:339–47. https://doi.org/10.1016/j.jnucmat.2015.04.001.
[44] Marinelli G, Martina F, Ganguly S, Williams S, Lewtas H, Hancock D, et al. Microstructure and thermal properties of unalloyed tungsten deposited by wire + Arc Additive Manufacturing. J Nucl Mater 2019;522:45–53. https://doi.org/10.1016/j.jnucmat.2019.04.049.
[45] ASTM International, ASTM Standard E1461-13. Standard Test Method for Thermal Diffusivity by the Flash Method. 2013. https://doi.org/10.1520/E1461-13.
[46] De Shan Z, Ye YS, Zhang ML, Wang BY. Hot-stamping die-cooling system for vehicle door beams. Int J Precis Eng Manuf 2013;14:1251–5. https://doi.org/10.1007/s12541-013-0170-3.
[47] Lin T, Song HW, Zhang SH, Cheng M, Liu WJ. Cooling systems design in hot stamping tools by a thermal-fluid-mechanical coupled approach. Adv Mech Eng 2014;2014. https://doi.org/10.1155/2014/545727.
[48] Lv M, Gu Z, Li X, Xu H. Optimal Design for Cooling System of Hot Stamping Dies. ISIJ Int 2016;56:2250–8. https://doi.org/10.2355/isijinternational.isijint-2016-191.
[49] Choi J, Chang Y. Characteristics of laser aided direct metal/material deposition process for tool steel. Int J Mach Tools Manuf 2005;45:597–607. https://doi.org/10.1016/j.ijmachtools.2004.08.014.

Magdalena Cortina is a full-time researcher at the Department of Mechanical Engineering of the University of the Basque Country (UPV/EHU) since 2016. Currently, she is finishing her PhD, which is focused on the application of the Directed Energy Deposition process to hot stamping tools, as well as on the study of hybrid manufacturing combining additive and subtractive technologies. This research work has resulted in five indexed publications and several contributions to national and international conferences.

Jon Iñaki Arrizubieta is Associate Professor at the University of the Basque Country (UPV/EHU) since 2018. He completed his PhD in the field of laser additive processing and is currently an active member of the High Performance Manufacturing Group and is also attached to the Aeronautics Advanced Manufacturing Center (CFAA). His work is focused on the repair of high-added-value parts by laser additive manufacturing, focusing mainly on the aeronautical and automotive sectors. He currently has more than ten relevant publications in indexed journals, as well as contributions at national and international conferences. He also participates in various international funded projects.

Jose Exequiel Ruiz finished his masters in Mechanical Engineering in 2015 and is currently working on his PhD. He is a researcher at the Department of Mechanical Engineering of the University of the Basque Country (UPV/EHU), and his studies are focused on the Laser Metal Deposition process with highly reactive materials and nickel-based alloys for the aeronautical industry. His research works have led to two indexed publications and national and international conference presentations.

Aitzol Lamikiz is Full Professor of Mechanical Engineering at the University of Basque Country (UPV/EHU). His current research interest includes metal additive manufacturing, laser material processing and process modelling. At present, he is working on laser material deposition, laser hardening and laser texturing processes, and collaborates on machining process modelling and monitoring. He has more than 15 years of experience in lecturing and researching on manufacturing processes. He has published more than 80 research papers on high impact international journals and a h-index 30. He leads several European, Spanish and Basque regional funded research projects.